

The Effects of Scintillation on Non-Redundant Aperture Masking Interferometry¹

Lewis C. Roberts, Jr., L. William Bradford, Mark A. Skinner

The Boeing Company, 535 Lipoa Pkwy, Suite 200, Kihei, HI 96753, lewis.c.roberts@boeing.com, lawrence.w.bradford@boeing.com, mark.a.skinner@boeing.com

Theo A. ten Brummelaar, Nils H. Turner

The CHARA Array, PO Box 48, Mount Wilson CA 91023, theo@chara-array.org, nils@chara-array.org

Ben R. Oppenheimer, Andrew P. Digby

Department of Astrophysics, American Museum of Natural History 79th Street at Central Park West New York, NY 10024, bro@amnh.org, apd@amnh.org

Marshall D. Perrin

University of California, Berkeley, Department of Astronomy, 601 Campbell Hall, Berkeley, CA 94720, perrin@astro.berkeley.edu

ABSTRACT

y-

Non-redundant aperture masking is a form of interferometry, where the aperture of the telescope is divided into two or more sub-apertures. There is no need for path length equalization or the other complex equipment that is required for long-baseline interferometry. The light from these subapertures interferes and details of the shape of the object can be determined by analyzing the resulting fringe patterns. While using such a mask does reduce the sensitivity of the optical system, it vastly improves the direct knowledge of the point spread function, thereby allowing much higher quality images.

We have collected pupil images with the AEOS telescope and use these real data to simulate the effects that variations in the amplitude of the incoming wavefront (*ie.* scintillation) have on the visibility measured by a two-element aperture system. We find that scintillation has little effect on observations taken above 60 degrees elevation and what little effect there is can be effectively calibrated. At low elevations, the effects are more significant and harder to calibrate. Scintillation

¹Based on observations made at the Maui Space Surveillance System operated by Detachment 15 of the U.S. Air Force Research Laboratory's Directed Energy Directorate.

will have little effect on most astronomical imaging situations, but it will be a problem if the technique is used to observe fast moving low-Earth satellites.

1. INTRODUCTION

Non-redundant Aperture Masking (NRM) has been used over the past twenty years for astronomical observations. It has been used to study binary stars(1), giant stars(2) and to create images of complex dust shells(3).

The effects of phase aberrations have been analyzed and techniques for calibrating these aberrations are well established, but the effects of amplitude variations have not been studied. Tango(4) studied the effects of scintillation on long-baseline interferometers, but that is largely irrelevant to the aperture masking. To understand the impact of scintillation, we took a series of pupil images with the AEOS telescope and used them to create simulated aperture masking data sets.

Visibility amplitude measurements need to be calibrated for seeing and instrumental response by observations of unresolved stars. These stars are normally observed at similar elevations to the science target. The visibility of an unresolved object is equal to one at all baselines, so the observation of a point source will yield its visibility multiplied by the visibility degradation. This technique works well except that the seeing can often change between the science observation and the calibration observation even in the course of a few minutes. This provides visibility errors of 5-10% (2; 5).

In the past the effects of scintillation have not be considered because scintillation is a minor problem for astronomical observations in general, where the observations are taken at high elevation angles. In general, this assumption has proven to be a good one. Scintillation can not be so easily ignored for observations of other object classes such as artificial satellites. For satellites in low-Earth orbit, the observations can start as soon as the object clears the horizon and the elevation angle of the culmination of the orbit can span 0° to 90° . Geo-stationary satellites are at fixed locations in the sky, but not necessarily a very high elevation angle. The impact of scintillation must be considered in these more challenging observations.

2. DATA COLLECTION

As part of a larger effort to understand atmospheric scintillation(7; 8), we collected images of the pupil of the AEOS 3.6 m telescope located at the Maui Space Surveillance System on Haleakala, Maui. To do this we modified the Lyot Project coronagraph(6). The coronagraph is designed to detect exo-solar planets with the use of the AEOS Adaptive Optics (AO) system. Normally a video-rate CCD camera observes the Lyot mask which is at a pupil. We inserted a flat mirror in front of this mask, which enabled us to collect pupil images, and a filter wheel so that we could

select the observation bandpass. All of the data presented in this paper were taken with an *I*-band filter and are 176×180 pixels. The pixels are square with each side being $9 \mu\text{m}$ across. The extent of the illuminated pupil is approximately 116 pixels. The camera collects data at 30 Hz, but we were unable to store every frame due to the inability of the hard disks to keep up with the data collection. Furthermore the data collection rate decreases as the number of files in each directory increases. Each data set consisted of 1000 frames, though occasionally multiple data sets were collected on a given star.

For each data set, we acquired a star with the AO system and sent the beam into the coronagraph which was set up in one of the experiment rooms located in the first floor of the AEOS building. While the beam passes through the AO system, we did not turn on the AO system. We did experiment with turning on the tip/tilt system, but we did not see any change in the data and for the most part the data were taken completely open loop.

We collected data on the nights of 7-8 June 2004. We had planned on observing stars at a variety of elevations and azimuths, but partway through the first night of observations, the winds exceeded 20 mph and the dome walls were raised to protect the telescope, which limited our viewing angle to 60° above the horizon. (The AEOS telescope has a non-traditional dome design which lowers and fully exposes the telescope to the ambient air.) We had only observed a single star lower than 60° before the dome walls had to be raised. The winds continued to be above 20 mph for the remainder of the observing run. All the observed stars had visual magnitudes brighter than 3.0.

For the data reduction, we masked off each image where there was no incoming light. This includes the areas outside of the pupil, but also the secondary mirror supports and the secondary shadow. Next, we averaged each data set of 1000 frames together. This creates an intensity map of the AEOS pupil. It differs from unity due to a number of factors including variations in mirror coatings, and actuator print through from both the AEOS primary mirror, which has an active optics system, and deformable mirror of the AEOS AO system. Also, at the time of the observations, the deformable mirror had several broken actuators, one of which was stuck in a negative position, resulting in a zero in the intensity map. Each image in the data set is then divided by this intensity map. This also acts a flat field and removes responsivity variations in the camera.

3. SIMULATIONS

We used the reduced data sets to help determine the impact of scintillation on aperture masking observations through a series of simulations. We created an aperture mask scaled to the AEOS primary with two sub-apertures 15 cm in diameter. The centers of the sub-apertures were separated by three meters. The mask was set to one in the sub-apertures and zero everywhere else. Each of the 1000 frames in each data set of pupil images was then multiplied by the mask. Next, we took the square root of the masked image, since we are interested in the amplitude of the incoming wave, not the recorded intensity. We then computed the power spectra of each masked image and

summed the power spectra of the individual frames for the entire data set. We computed the square of the visibility (V^2) from the combined power spectra of the data set. We also computed the power spectrum of a masked pupil with no scintillation and used this to normalize each of the measured V^2 .

This is equivalent to observing a point source with only scintillation affecting the measurement of the V^2 . There are no phase variations in this simulation, which allows us to isolate the effects of scintillation. If scintillation had no effect on aperture masking observations, then the V^2 would be 1.0.

4. RESULTS

In Fig. 1 we show the time history of the V^2 for the star HR 7635, which was observed at an elevation of $87^\circ.4$. The average V^2 is 0.99 with a standard deviation of 0.040. Compare this with Fig. 2. This shows the time history of the V^2 of HR 3982 which was observed at an elevation of $13^\circ.2$. The scintillation is much higher for this data set, as is to be expected for observations through this much airmass. The average V^2 is 0.93 with a standard deviation of 0.10. Not only is the impact of scintillation now significant, it is also highly variable. Table 1 gives the Bright Star Catalog number of the star, as well as the UT date, elevation, V^2 , and the average scintillation index of the unmasked data frames. Higher scintillation indices are found at lower elevations as is to be expected.

In both graphs, there are V^2 data with values higher than 1.0. This is non-intuitive, but real data show this same behavior. The coherence of the two wavefronts depends on several things. First, and most importantly there is the coherence derived from the topology of the source itself, the very thing we'd like to measure. This is modified by many other things, including atmospheric phase aberrations and scintillation, as well as instrumental effects such as AO system induced phase effects and detector instability. These some times add to and sometimes subtract from the real object coherence. The visibility amplitude can therefore be considered to be a Gaussian random variable with the mean of the coherence, or V^2 , and a standard deviation which depends on the numerous things impacting the coherence. Thus, if the mean coherence is one, we must expect that individual measures of the coherence will sometimes be greater than and sometimes less than one, otherwise the mean can not be one. The same conclusion holds if the mean is zero, that is, in a real instrument it is entirely possible for a measurement of V^2 to be less than one.

In Fig. 3 we show the V^2 for the summed power spectra of each data set as a function of elevation. The data sets taken at low elevations have relatively large reductions in V^2 . Since we only have two data sets taken at low elevations, we are unable to determine at which elevation the reduction in V^2 becomes significant, or even the shape of the curve. Additional data is required to fully answer this. Still the graph provides enough information to determine that at elevations above 60° , it is fairly simple to calibrate the effects of scintillation out from aperture masking data. Even

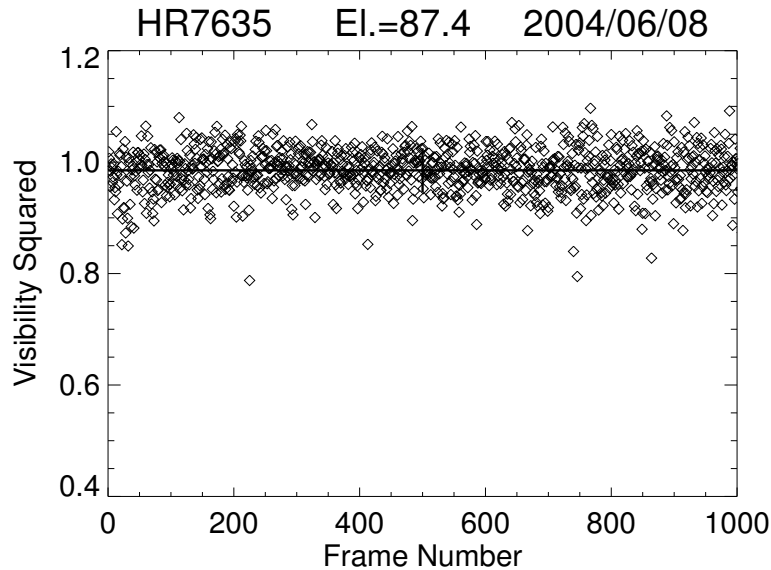


Fig. 1.— The visibility squared (V^2) as a function of frame number for the star HR 7635 which was observed at an elevation angle of 87° above the horizon. The horizontal line is the average of the V^2 , 0.99, while the vertical line is plus or minus the standard deviation of the V^2 , 0.040. Compare this to Fig. 2 which is acquired a much lower elevation angle and is plotted on the same scale.

though the data sets were taken over two nights their respective V^2 values are very close, even for data taken with differences of 20° in elevation. Some of the data sets were taken of the same star in sequence. This would be the fastest any calibration data set could be taken. There are small differences in the measured V^2 ; for instance, we observed HR 7235 three times and the measured values are: 0.7837, 0.7876, and 0.7903. The differences are very small and would have no measurable impact on the analysis. This shows that the usual astronomical calibration scheme of observing a nearby calibrator star after a science observation will work quite well for calibrating scintillation.

Data for these stars were also taken at different azimuth locations which also does not cause large variations in V^2 . This agrees with measurements of the scintillation index, which also do not vary with azimuth. In addition, we reran the simulations with a variety of sub-aperture separations and the V^2 showed no dependency on separation.

5. CONCLUSIONS

We have shown that scintillation has minimal impact on the measured V^2 from aperture masking observations for stars observed above 60° elevation. For stars at low elevations, there is significant degradation to the V^2 from the scintillation. Even so, it can be calibrated out by observing a nearby

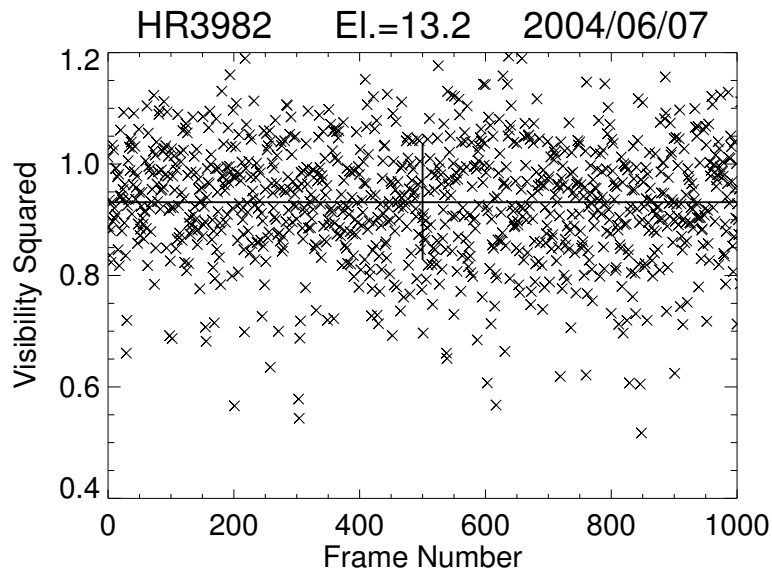


Fig. 2.— The visibility squared (V^2) as a function of frame number for the star HR 3982 which was observed at an elevation angle of 13.2° above the horizon. The horizontal line is the average of the V^2 , 0.93, while the vertical line is plus or minus the standard deviation of the V^2 , 0.1.

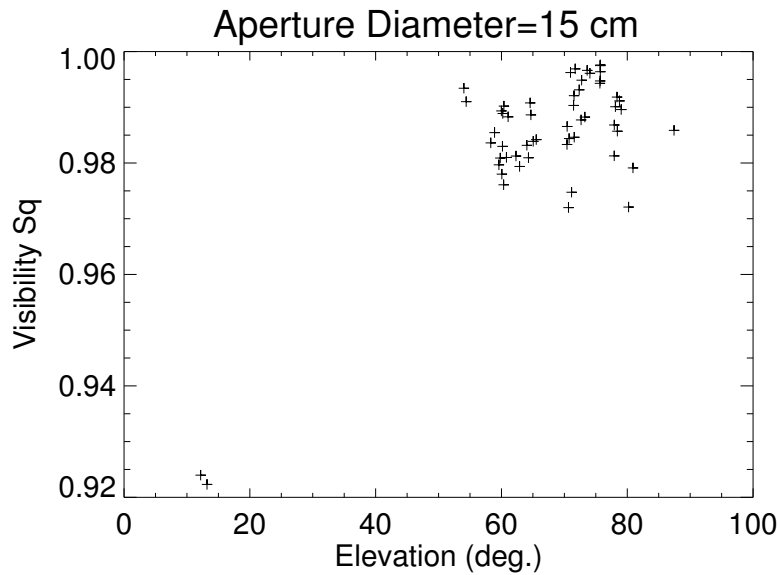


Fig. 3.— This shows the visibility squared (V^2) as a function of elevation angle of the observed star. For stars above 60° there is little degradation due to scintillation. At low elevations, there is a significant amount of visibility loss, which is attributed to the increased scintillation index.

calibrator star. This will work quite well for observations of stars and other astronomical objects, where the object moves slowly through the sky. It will also work well for observations of geosynchronous satellites, which move even slower through the sky. The one area where calibration will pose difficult is the observation of satellites in low-Earth orbits. These satellites move from horizon to horizon in the matter of minutes. Since these objects change elevation angles in a short period of time, it will require more calibrator stars at low elevations to properly calibrate out the effects of scintillation. To finalize these conclusions and to assess the impact of not enough calibration stars, we need to collect additional data sets filling in the missing elevation angles. We hope to do that in the coming months.

6. Acknowledgments

Anand Sivaramakrishnan provided useful and friendly advice on our simulations. We thank the staff members of the Maui Space Surveillance System for their assistance in taking these data. This research was funded by the Air Force Office of Scientific Research through AFRL/DE (Contract Number F29601-00-D-0204) and by the National Science Foundation through grants AST-0088316 and AST-0215793. B.R. Oppenheimer was partially supported by the American Museum of Natural History's Kalbfleisch Fund. A.P. Digby and M.D. Perrin were supported by NASA Michelson Fellowships under contract to the Jet Propulsion Laboratory funded by NASA.

REFERENCES

1. T. Nakajima, S.R. Kulkarni, P.W. Gorham, A.M. Ghez, G. Neugebauer, J.B. Oke, T.A. Prince & A.C.S Readhead, "Diffraction-Limited Imaging. II Optical Aperture-Synthesis Imaging of Two Binary Stars", *Astron. J.*, **97**, 1510–1525 (1989).
2. R.W. Wilson, J.E. Baldwin, D.F. Buscher, & P.J. Warner, "High-Resolution Imaging of Betelgeuse and Mira", *Mon. Not. R. Astron. Soc.*, **257**, 369–376 (1992).
3. P.G. Tuthill, J.D. Monnier, W.C. Danchi, E.H. Wishnow, & C.A. Haniff, "Michelson Interferometry with the Keck I Telescope", *Publ. Astron. Soc. of the Pac.*, **112**, 555–565 (2000).
4. W.J. Tango, "Scintillation in Optical Stellar Interferometry", *Publ. Astron. Soc. of the Pac.*, **110**, 995–998 (1998).
5. R.W. Wilson, V.S. Dhillon, & C.A. Haniff, "The Changing Face of Betelgeuse", *Mon. Not. R. Astron. Soc.*, **291**, 819–826 (1997)
6. B.R. Oppenheimer, A.P. Digby, L. Newburgh, M. Shara, D. Brenner, A. Sivaramakrishnan, R.B. Makidon, R. Soummer, J.P. Lloyd, J.R. Graham, P. Kalas, M. Perrin, J.R. Kuhn, K. Whitman, & L.C. Roberts, Jr., "The Lyot Project: toward exoplanet imaging and spectroscopy" *Proc. SPIE*, **5490**, 433–442 (2004).

7. L.W. Bradford, L.C. Roberts, Jr., M.A. Skinner, A.P. Digby, B.R. Oppenheimer, M.D. Perrin, & N.H. Turner, "Observations of Scintillation at AEOS" Proc. of AMOS Conf., 471–491 (2005).
8. A. Sivaramakrishnan, B.R. Oppenheimer, M.D. Perrin, L.C. Roberts, Jr., R.B. Makidon, R. Soummer, A.P. Digby, L.W. Bradford, M.A. Skinner, N.H. Turner, T.A. ten Brummelaar, "Direct Imaging of Exoplanets: Science & Techniques. Proc. of the IAU Colloquium #200," Edited by C. Aime and F. Vakili. Cambridge, UK: Cambridge University Press, 613–616, (2006).

Table 1. This table presents the stars that were observed along with the associated elevation angles, V^2 , and the average scintillation index for the unmasked data set.

BSC	UT Date (m/d)	El. ($^{\circ}$)	V^2	σ_I
3982	6/7	13.2	0.922	0.0257
	6/7	12.2	0.924	0.0508
4932	6/7	72.4	0.993	0.0037
5854	6/7	75.7	0.995	0.0040
	6/7	75.7	0.996	0.0003
	6/7	75.7	0.998	0.0003
	6/7	75.7	0.997	0.0004
	6/7	75.7	0.994	0.0013
	6/7	72.7	0.995	0.0009
	6/7	71.7	0.997	0.0013
	6/7	71.0	0.996	0.0015
6536	6/7	54.0	0.993	0.0108
	6/7	54.4	0.991	0.0036
	6/7	74.1	0.996	0.0010
	6/7	73.6	0.997	0.0011
6212	6/8	60.1	0.978	0.0098
	6/8	59.6	0.980	0.0088
6556	6/8	73.3	0.988	0.0087
	6/8	72.7	0.988	0.0134
7001	6/8	71.5	0.992	0.0157
	6/8	71.6	0.985	0.0082
7235	6/8	78.3	0.992	0.0037
	6/8	78.8	0.991	0.0035
	6/8	79.0	0.990	...
	6/8	71.1	0.975	0.0128
	6/8	70.7	0.972	0.0426
	6/8	60.8	0.981	0.0202
	6/8	60.3	0.976	0.0554
	6/8	60.3	0.976	0.0554
7525	6/8	77.9	0.987	0.0220
	6/8	78.4	0.986	0.0185
	6/8	80.9	0.979	0.0158
	6/8	80.2	0.972	0.0209
7557	6/8	78.1	0.990	0.0145

Table 1—Continued

BSC	UT Date (m/d)	El. ($^{\circ}$)	V^2	σ_I
	6/8	77.9	0.981	0.0203
7635	6/8	87.4	0.986	0.0213
7796	6/8	65.0	0.984	0.0230
	6/8	65.5	0.984	0.0165
	6/8	70.4	0.987	0.0122
	6/8	70.4	0.983	0.0173
7924	6/8	64.7	0.989	0.0079
	6/8	64.6	0.991	0.0128
7949	6/8	62.3	0.981	0.0101
	6/8	62.9	0.979	0.0228
	6/8	70.8	0.984	0.0206
	6/8	71.5	0.990	0.0060
8232	6/8	60.0	0.989	0.0210
	6/8	60.2	0.989	0.0185
8414	6/8	60.4	0.990	0.0120
	6/8	61.1	0.988	0.0246
8650	6/8	64.0	0.983	0.0111
	6/8	64.3	0.981	0.0770
8775	6/8	58.3	0.984	0.0149
	6/8	58.9	0.985	0.0240
8781	6/8	59.8	0.981	0.0752
	6/8	60.2	0.983	0.0444